Journal Pre-proof

Improved mechanical properties of high-speed extruded BA53 alloy through long-range water-cooling system

Sang-Cheol Jin, Jae Won Cha, Hyun Ji Kim, Jeong Hun Lee, Hui Yu, Sung Hyuk Park

PII: S2238-7854(24)00028-0

DOI: https://doi.org/10.1016/j.jmrt.2024.01.028

Reference: JMRTEC 9661

To appear in: *Journal of Materials Research and Technology*

Received Date: 1 December 2023

Revised Date: 4 January 2024

Accepted Date: 4 January 2024

Please cite this article as: Jin S-C, Cha JW, Kim HJ, Lee JH, Yu H, Park SH, Improved mechanical properties of high-speed extruded BA53 alloy through long-range water-cooling system, *Journal of Materials Research and Technology* (2024), doi: https://doi.org/10.1016/j.jmrt.2024.01.028.

Improved mechanical properties of high-speed extruded BA53 alloy through long-range water-cooling system

Sang-Cheol Jin[a], Jae Won Cha[a], Hyun Ji Kim[a], Jeong Hun Lee[b], Hui Yu[c], Sung Hyuk Park[a,*]

[a] *School of Materials Science and Engineering, Kyungpook National University, Daegu 41566, Republic of Korea*

[b] *Ulsan Regional Division, Korea Institute of Industrial Technology, Ulsan 44413, Republic of Korea*

[c] *School of Materials Science and Engineering, Hebei University of Technology, Tianjin, 300130, China*

*Corresponding author. *E-mail*: sh.park@knu.ac.kr (S.H. Park).

Abstract

A recently developed Mg–5Bi–3Al (BA53, wt%) alloy exhibited remarkable extrudability despite its high alloying content. However, when subjected to high-speed extrusion with a die exit speed of 67 m/min, grain coarsening of recrystallized grains occurs, increasing their size from 12.1 to 26.4 μm due to excessive heat generation during extrusion. Herein, a long-range water-cooling system is installed immediately after the extrusion die to mitigate grain coarsening and attain finer grains in the high-speed extruded alloy. The results demonstrate that the use of the cooling system leads to a significant reduction in the average

grain size (from 26.4 to 15.7 μm) of the BA53 alloy extruded at high speed. Furthermore, grain refinement led to notable increases in the ultimate tensile strength (from 255 to 276 MPa) and elongation (from 7.5% to 8.6%) of the alloy. These enhancements in strength and elongation are primarily attributed to the enhanced grain-boundary hardening effect and suppression of twinning during tension, both of which are consequences of grain refinement. This study underscores the effectiveness of a long-range water-cooling system, comprising water spraying over a length of 2 m, in achieving grain refinement during high-speed extrusion of the BA53 alloy and improving both the strength and ductility of the alloy after high-speed extrusion.

Keywords

Magnesium alloy; Extrusion; Water cooling; Microstructure; Mechanical properties

1. Introduction

Mg alloys, characterized by low density, high strength-to-weight ratio, and excellent damping capacity, have emerged as compelling candidates for a wide range of applications in various industries, such as aerospace, automotive, and electronics, where weight reduction and improved energy efficiency are of paramount importance [1–7]. Notably, wrought Mg alloys subjected to hot metal–forming processes exhibit a finer grain structure and better mechanical properties than cast Mg alloys, thus entailing the applicability of the former across a broader range of industries. Extrusion and rolling are the most widely used metal-forming processes. Compared with rolling, which requires multiple operation passes and intermediate heat treatment, extrusion enables easier manufacturing of complex-shaped products in a single pass [7,8]. In addition, dynamic recrystallization (DRX) and/or dynamic precipitation occur vigorously during the hot extrusion of Mg alloys because of the high strain that the material undergoes, improving the mechanical properties of the extruded material.

High-Al-containing Mg alloys (e.g., AZ61, AZ80, and AZ91), which are representative commercial Mg alloy systems, exhibit high castability and strength. However, they have poor extrudability due to the low melting point (437 °C) of the $Mg_{17}Al_{12}$ phase formed in Mg–Al-based alloys [9]. Jin et al. [10] reported that the extrusion of an AZ80 alloy at 400 °C and an extrusion ratio of 50 results in severe hot cracking at an exit die speed of 4.5 m/min, indicating that the maximum extrusion speed of this alloy is below 4.5 m/min. To overcome the limited extrudability of commercial Mg alloys with high alloying contents, Mg–Bi–Al alloys

that can be extruded at high speeds have been recently developed [10–17]. In the Mg–Bi–Al alloys, Bi forms a Mg_3Bi_2 phase with a high melting point (823 °C), enabling high-speed extrusion, and Al is dissolved in the Mg matrix, promoting DRX during extrusion and increasing the strength of the extruded material. A recent study [12] demonstrated the outstanding extrudability of the Mg–5Bi–3Al (BA53, wt%) alloy, with a maximum extrusion speed of >70 m/min despite a high alloying content (8.0 wt%). Moreover, the BA53 alloy extruded at high speed exhibits relatively high strength due to the presence of fine Mg_3Bi_2 particles.

One of the primary concerns in the high-speed extrusion of BA53 alloy is the coarsening of dynamically recrystallized (DRXed) grains, which is driven by excessive heat generation during high-speed extrusion. This grain coarsening reduces the mechanical properties of the material, potentially limiting its practical applications. Accordingly, there is a pressing need to explore effective techniques that could not only mitigate grain coarsening but also enhance the strength and ductility of the alloy. Herein, this critical issue is addressed using a long-range water-cooling system. The cooling system was installed immediately after the extrusion die exit to suppress grain coarsening in the high-speed extruded BA53 alloy. This study refined the microstructure of the alloy, thereby improving its mechanical properties. A comprehensive analysis of the effects of this cooling system on the microstructure and tensile properties of the extruded material is expected to contribute to technological advancements in the fabrication of high-performance Mg alloys at high processing speeds, which can expand their industrial applications.

2. Experimental procedure

Two BA53 alloy billets were prepared through conventional mold casting; details of the casting process can be found in a previous study [10]. The cast billets were homogenized at 450 °C for 10 h, followed by water quenching. The homogenized billets were machined to a cylindrical shape with dimensions of 68 mm (diameter) × 120 mm (length). High-speed extrusion was performed at 400 °C, ram speed of 14.6 mm/s, and extrusion ratio of 76.5; the exit speed of the extruded material was 67 mm/min. One billet was extruded naturally air-cooled without artificial cooling; therefore, this material is hereafter referred to as the naturally cooled (NC) material. The other billet was artificially cooled using a long-range water cooling system. As shown in Fig. 1, immediately after the material exits the extrusion die, it passes through a cooling section where water is sprayed over a length of 2 m. This material is hereafter the artificially cooled (AC) material.

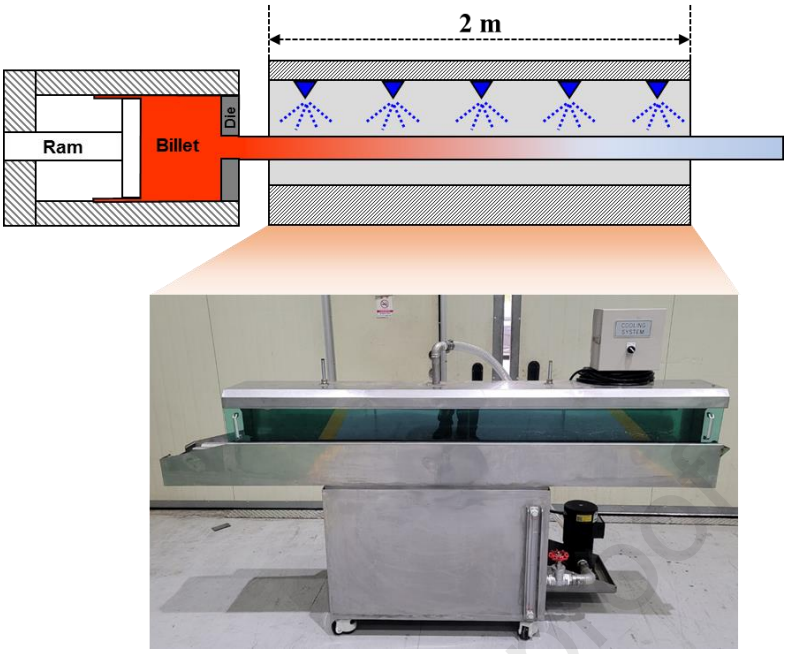

Fig. 1. Schematic and photo of extrusion with long-range water-cooling system.

The microstructures of the cross-section along the extrusion direction (ED) of the two high-speed extruded BA53 materials (i.e., NC and AC materials) were analyzed using optical microscopy, field-emission scanning electron microscopy (SEM), and electron backscatter diffraction (EBSD). Details of sample preparation for measuring the microstructure can be found in a previous study [13]. The grain size distributions, (0001) pole figures, ED inverse pole figures (IPFs), IPF maps, Schmid factor (SF) maps, and grain orientation spread (GOS) maps of the NC and AC materials were obtained from reliable EBSD data (confidence index values of >0.1). Cylindrical dogbone-shaped tensile specimens with gage dimensions of 5 mm (diameter) × 25 mm (length) were machined from the extruded materials according to the ASTM E8 standard. Uniaxial tensile testing was conducted at room temperature (25 °C) and a strain rate of 1.0×10^{-3} s^{-1}. The tensile testing was carried out three times for each material, and the

tensile properties were determined by averaging the test results. The microstructure and fracture surface of the specimens after tensile testing were observed using optical microscopy and SEM.

3. Results

Figs. 2a and b show the IPF maps of the high-speed extruded BA53 alloys produced with and without the long-range water-cooling system, respectively. The average grain size of the NC material, which was naturally air-cooled after exiting the extrusion die, is 26.4 μm, whereas that of the AC material, which was artificially water-cooled immediately after exiting the extrusion die, is 15.7 μm. This indicates that the long-range water-cooling system is effective in reducing the grain size of extruded Mg alloys even at an extremely high extrusion speed of 67 m/min. During the extrusion of the BA53 alloy at 400 °C and extrusion ratio of 76.5, its microstructure in the deformation zone near the extrusion die changes into DRXed grains because of sufficient thermal and deformation energies for complete DRX [13,14,18,19]. Once the material exits the extrusion die, it is no longer subjected to deformation, causing static grain growth during cooling to reduce the internal strain energy of the material [19–21]. To determine the degree of static grain growth that occurred during air and water cooling, the grain size at the die exit was measured by observing the microstructure of the extrusion butt remaining after extrusion (Fig. 2c). The grain size measured at the die exit is 12.1 μm, meaning that the grain size increases by 118% (to 26.4 μm) during natural air-cooling and by only 30% (to 15.7 μm) during artificial water-cooling.

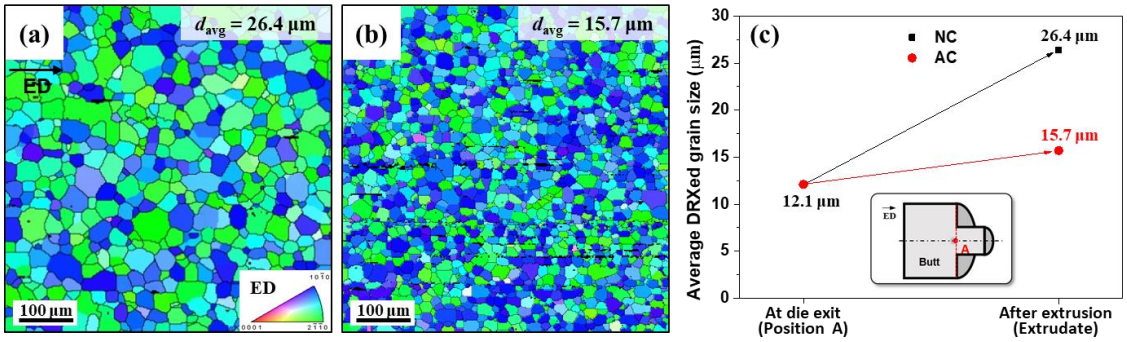

Fig. 2. Inverse pole figure maps of high-speed extruded BA53 alloys: (a) naturally cooled (NC) and (b) artificially cooled (AC) materials. (c) Average grain sizes of the materials at the die exit and after extrusion.

Figs. 3a and b show the SEM microstructures of the NC and AC materials, which exhibit that secondary phase particles are observed in both materials. The equilibrium phase diagram of the Mg–5Bi–*x*Al alloy calculated using FactSage software (Fig. 3c) reveals that at a homogenization temperature of 450 °C, the BA53 alloy comprises two phases, *α*-Mg and Mg_3Bi_2. This means that Mg_3Bi_2 particles in the cast billet of the BA53 alloy are not completely dissolved in the *α*-Mg matrix during homogenization at 450 °C. The remaining Mg_3Bi_2 particles in the homogenized billet are redistributed along the metal flow direction during extrusion. Owing to the considerably high strain applied during extrusion (4.34), some undissolved Mg_3Bi_2 particles are arranged in the form of a very long band parallel to the ED (yellow arrows in Figs. 3a and b). Since the extrusion temperature (400 °C) is lower than the homogenization temperature (450 °C), a small amount of Mg_3Bi_2 particles can be formed during extrusion. However, Mg_3Bi_2 particles are not readily formed during extrusion because the deformation

duration under the high-speed extrusion condition adopted in this study is insufficient for the dynamic precipitation of the Mg_3Bi_2 phase. Therefore, the NC and AC materials contain only Mg_3Bi_2 particles without any other phases such as $Mg_{17}Al_{12}$, and the area fraction and distribution of the particles are almost the same in the two materials.

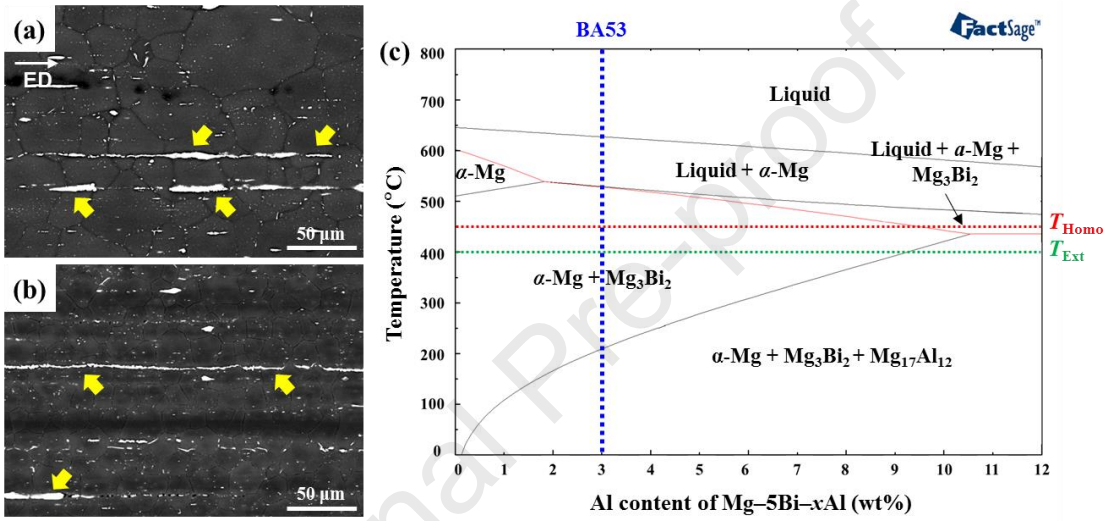

Fig. 3. SEM micrographs of longitudinal cross-sections of (a) NC and (b) AC materials. (c) Equilibrium phase diagram of Mg–5Bi–*x*Al (*x* = 0–12 wt%) calculated using FactSage software.

The engineering tensile stress–strain curves with the average tensile properties of the NC and AC materials are shown in Fig. 4. The tensile yield strength (TYS) and ultimate tensile strength (UTS) of the NC material are 198 and 255 MPa, respectively, and those of the AC material are 208 and 276 MPa, respectively. Hence, the TYS and UTS of the AC material are higher than those of the NC material by 10 and 21 MPa, respectively. In addition, the total elongations of the NC and AC materials are 7.5% and 8.6%, respectively,

indicating that the tensile ductility of the AC material is approximately 15% higher than that of the NC material. These results demonstrate that the application of the long-range water cooling immediately after high-speed extrusion results in simultaneous improvements in the strength and ductility of the extruded BA53 alloy.

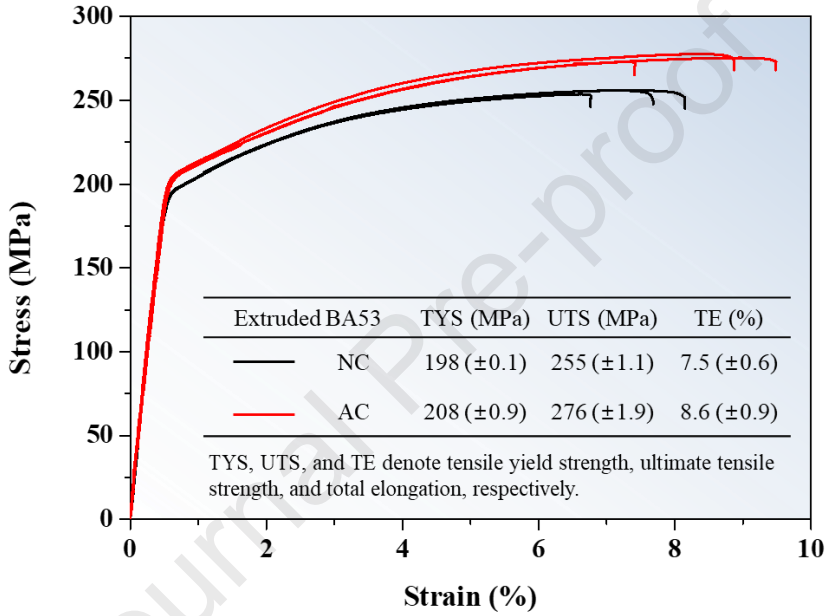

Fig. 4. Engineering tensile stress–strain curves with average tensile properties of NC and AC materials.

4. Discussion

The tensile strength of extruded Mg alloys is determined by a combination of solid-solution, secondary particle, texture, strain, and grain-boundary hardening effects [22–24]. As the NC and AC materials have the same alloying compositions and contain similar amounts of Mg_3Bi_2 particles, the solid-solution and particle

hardening effects for the two materials are nearly identical. The (0001) pole figures, ED IPFs, and SF maps and distributions for the basal slip of the NC and AC materials are shown in Fig. 5. Both materials exhibit a typical basal texture with most basal poles arranged nearly perpendicular to the ED, as shown in their (0001) pole figures. Moreover, the maximum IPF intensities of the NC and AC materials are similar (5.0 and 5.3, respectively), and their average SF values for basal slip under the applied tension are the same (0.12). These results indicate that the effect of the long-range water-cooling system on the texture of the high-speed extruded BA53 alloy is insignificant; therefore, the NC and AC materials exhibit similar texture hardening effects during tension.

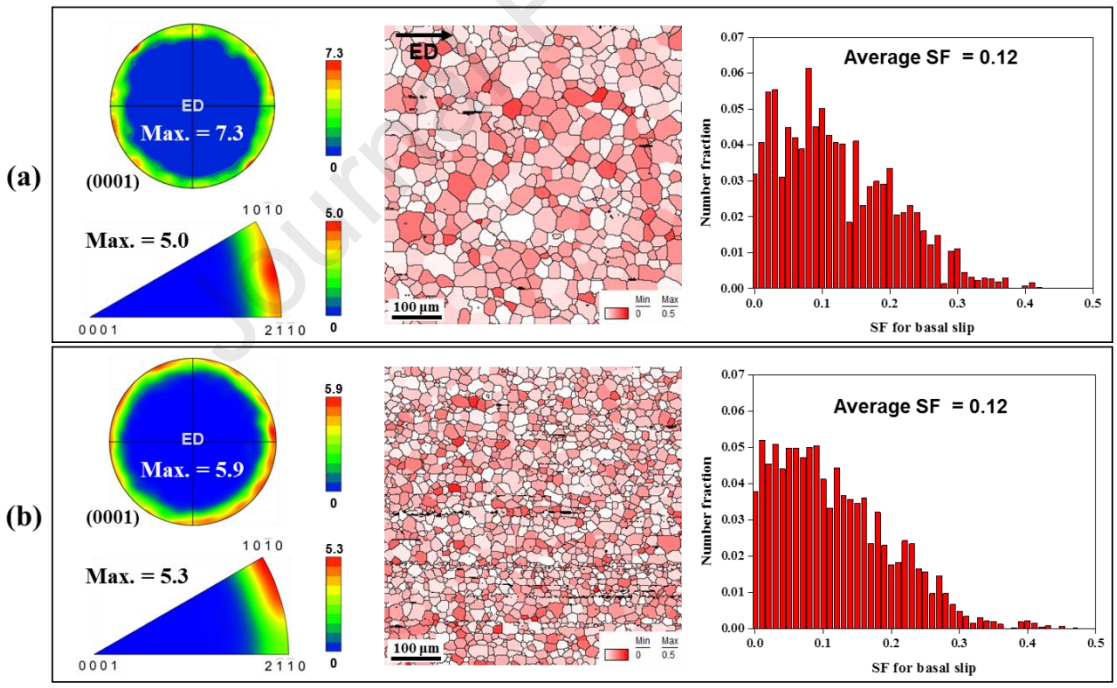

Fig. 5. (0001) pole figures, extrusion direction (ED) inverse pole figures, and Schmid factor (SF) maps and distributions for basal slip of (a) NC and (b) AC materials.

The strain hardening effect of a material is proportional to the square root of its dislocation density [25], and the dislocation density is directly proportional to the average GOS value obtained by EBSD [26]. Accordingly, the average GOS value of a material is commonly used as an indicator of its strain hardening effect [26,27]. As the NC and AC materials exhibit a fully DRXed grain structure due to complete DRX during extrusion, they possess low dislocation densities, as evidenced by their low average GOS values (Fig. 6). The threshold GOS value used to distinguish between DRXed and unDRXed grains is known as 1°–2° in various metallic materials [28–32], including Mg alloys [33,34]. In the GOS maps of the NC and AC materials, most grains appear in blue with a GOS value of <1°, suggesting that they are recrystallized grains formed in the late stage of extrusion [35]. In contrast, DRXed grains formed during the early stage of extrusion undergo deformation during extrusion, resulting in an increase in their GOS value. Hadazadeh et al. [35] reported that grains with GOS values between 2° and 5° in hot-deformed Mg alloys are deformed DRXed grains that underwent recrystallization during the initial stage of hot deformation. Hence, in the GOS maps of the NC and AC materials, grains that appear in green or yellow with a GOS of 2°–5° are considered to be deformed DRXed grains. The average GOS values of the NC and AC materials are 0.66° and 0.69°, respectively, which suggests similar strain hardening effects in the two materials. As the NC and AC materials exhibit similar solid-solution, particle, texture, and strain hardening effects, the higher tensile strength of the AC material is predominantly attributed to its stronger grain-boundary hardening effect. According to the Hall–Petch

equation, the relation between grain size and strength is as follows:

$$\sigma = \sigma_o + kd^{-1/2} \quad (1)$$

where σ_0 is the frictional stress, d is the grain size, and k is the Hall–Petch coefficient. Because the NC and AC materials have the same frictional stress and Hall–Petch coefficient, the strength increase caused by grain refinement via long-range water cooling can be derived from Eq. (1) as follows:

$$\Delta\sigma = k({d_{AC}}^{-1/2} - {d_{NC}}^{-1/2}) \quad (2)$$

where d_{AC} and d_{NC} are the average grain sizes of the AC and NC materials (15.7 and 26.4 μm), respectively. Our previous study [11] found that the extruded BA52 alloy has a Hall–Petch coefficient of 381.4 MPa·μm$^{-1/2}$. Assuming that the extruded BA53 alloy has the same Hall–Petch coefficient as the extruded BA52 alloy, the strength increase caused by grain refinement in the AC material is calculated to be 22.0 MPa from Eq. (2). This value is roughly consistent with the difference in the UTS values of the NC and AC materials (21 MPa). Therefore, the use of the long-range water-cooling system considerably decreases the grain size of the high-speed extruded BA53 alloy, resulting in an improvement in its tensile strength due to the enhanced grain-boundary hardening effect.

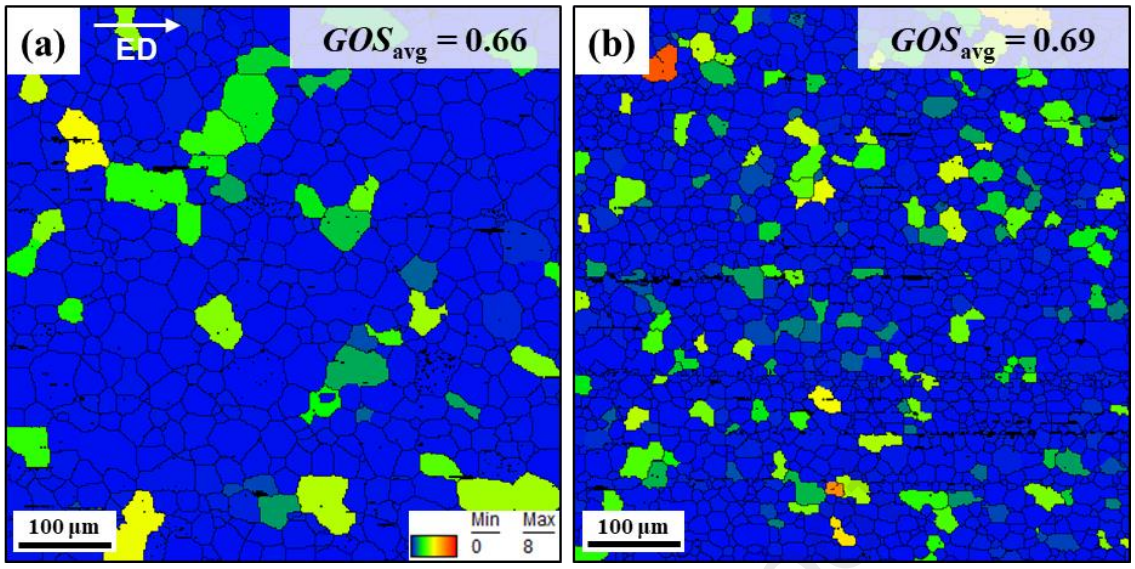

Fig. 6. Grain orientation spread (GOS) maps and average GOS values of (a) NC and (b) AC materials.

Although an increase in the strength of the material generally causes a decrease in elongation, the AC material exhibits a higher elongation than the NC material despite its higher strength. Fig. 7 shows the optical micrographs near the fracture line of the longitudinally cross-sectioned specimens after tensile testing. When extruded Mg alloys with a typical basal fiber texture are subjected to tension along the ED, {10-11} contraction twins and {10-11}-{10-12} double twins are formed, followed by the formation of cracks along the twins [36–38]. Although thin twins are observed in both the NC and AC materials, their number density is considerably higher in the AC material than in the NC material. As the stress for activating deformation twinning decreases with increasing grain size [39–41], contraction and double twins are more readily formed during tension in the NC material than in the AC material because of the larger grains of the former. Moreover, individual twins in the NC material are larger than those in the AC

material. The larger twins and subsequent cracking along the twins eventually lead to the formation of sharper fracture lines in the NC material (yellow arrows in Fig. 7a) compared with the AC material. Because of the smaller number density and larger size of the formed twins, the local stress concentration at the twins during tension is more pronounced in the NC material than in the AC material, resulting in the lower elongation of the former.

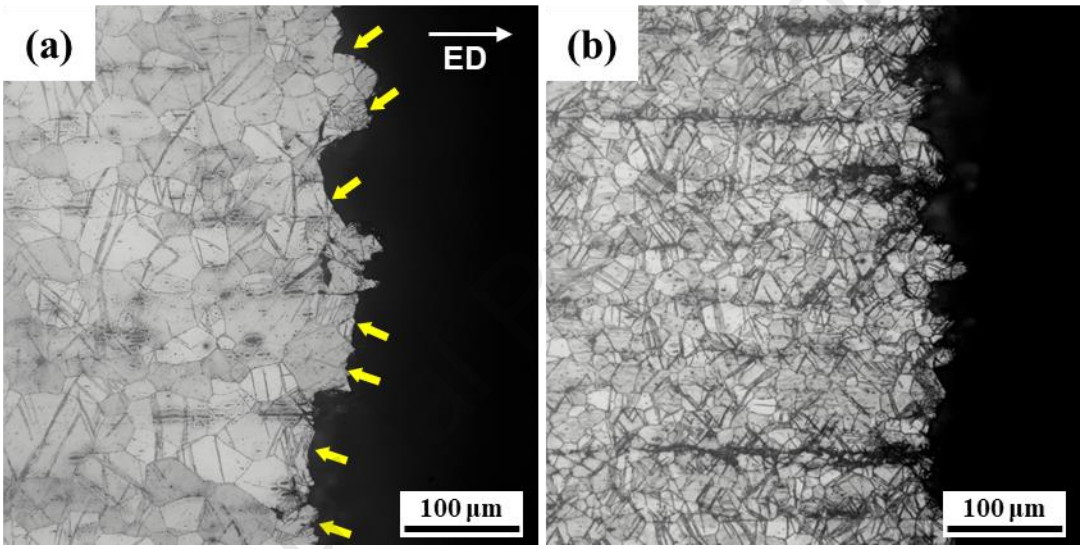

Fig. 7. Optical micrographs of longitudinal cross-sections of (a) NC and (b) AC materials after tensile testing.

The SEM fracture surfaces of the specimens after tensile testing and the grain size distributions before tension of the NC and AC materials are shown in Fig. 8. In both materials, several cleavage planes with river patterns are observed, which is consistent with previous results for extruded Mg alloys, in which tensile fracture occurs through cracking at twins [16,17,20,38]. The size of the cleavage planes formed in the NC material is approximately 35–65 μm. Although the average grain size of this material is 26.4 μm, large grains with a size of >30 μm

are present, with an area fraction of 33.1% (Fig. 8a). Because these large grains are favorable for twinning under tension, coarse cleavage planes with sizes similar to those of the grains are formed in the NC material. In contrast, the cleavage planes formed in the AC material have smaller sizes (17–30 μm) than those in the NC material because the area fraction of grains with a size of >30 μm in the former is considerably small (2.4%; Fig. 8b). Consequently, the improved strength and elongation of the AC material are primarily attributed to its refined grains formed during water cooling.

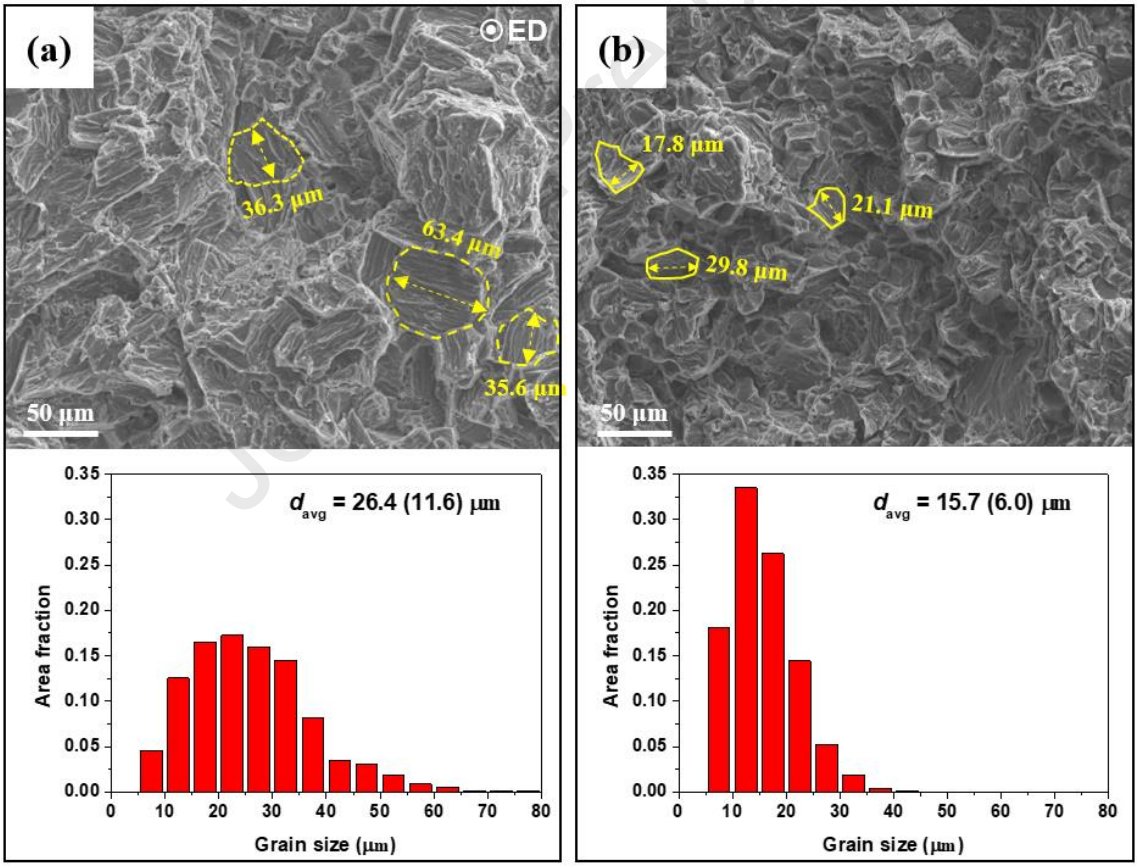

Fig. 8. SEM fractographs after tensile testing and grain size distributions before tension of (a) NC and (b) AC materials.

5. Conclusions

The recently developed BA53 alloy exhibits excellent extrudability. However, high-speed extrusion of this alloy with a die exit speed of 67 m/min leads to coarsening of the DRXed grains from 12.1 to 26.4 μm due to excessive heat generation during extrusion. To suppress grain coarsening during high-speed extrusion and obtain finer grains in the extruded alloy, a long-range water-cooling system is installed immediately after the extrusion die. The average grain size of the high-speed extruded BA53 alloy decreases from 26.4 to 15.7 μm through the application of the cooling system. In addition, its UTS and elongation increase from 255 to 276 MPa and 7.5% to 8.6%, respectively. The improvements in strength and elongation of the high-speed extruded BA53 alloy are primarily attributed to the enhanced grain-boundary hardening effect and suppressed twinning caused by grain refinement, respectively. This study demonstrates that cooling through spraying with water over a length of 2 m is effective for grain refinement of the high-speed extruded BA53 alloy, resulting in simultaneous increases in the strength and ductility of the extruded material.

Data availability

The raw/processed data required to reproduce these findings cannot be shared at this time, because the data also form part of an ongoing study.

CRediT authorship contribution statement

Sang-Cheol Jin: Methodology, Investigation, Formal analysis, Visualization, and Writing–original draft; **Jae Won Cha**: Methodology, Investigation, Formal analysis; **Hyun Ji Kim**: Investigation, Formal analysis; **Jeong Hun Lee**: Data curation, Investigation; **Hui Yu**: Conceptualization, Methodology; **Sung Hyuk Park**: Conceptualization, Formal analysis; Investigation, Writing–review and editing, Supervision, and Project administration.

Declaration of competing interest

The authors declare that they have no conflicts of interest.

Acknowledgments

This research was supported by the National Research Foundation of Korea (NRF) grant (No. 2019R1A2C1085272) funded by the Ministry of Science, ICT, and Future Planning (MSIP, South Korea) and by the Materials and Components Technology Development Program (No. 20024843) funded by the Ministry of Trade, Industry, and Energy (MOTIE, South Korea).

References

[1] F. Pan, M. Yang, X. Chen, A Review on Casting Magnesium Alloys: Modification of Commercial Alloys and Development of New Alloys, J. Mater. Sci. Technol. 32 (12) (2016) 1211–1221. https://doi.org/10.1016/j.jmst.2016.07.001.

[2] X. Wang, Y. Zhao, Y. Huang, Characterization of Hot-Extruded Mg–Gd–Y–Zn–Zr Alloy Containing a Novel Lamellar Structure and Related High Elevated-Temperature Mechanical Properties, Met. Mater. Int. 29 (2023) 2556–2570. https://doi.org/10.1007/s12540-023-01391-0.

[3] F.H. Gao, B.J. Lv, T.W. Xu, N. Cui, F. Guo, Effects of Sn and Mn Addition on the Microstructure and Mechanical Properties of As-Extruded Mg–2Al–1Zn Alloys, Met. Mater. Int. 29 (2023) 3178–9189. https://doi.org/10.1007/s12540-023-01435-5.

[4] L. Yang, Q. Li, X. Chen, W. Mei, N. Zhang, Effect of Ce Microalloying on Microstructure and Mechanical Properties of Extruded Mg–10Gd–0.5Zr Alloy, Met. Mater. Int. 29 (2023) 3190–3203. https://doi.org/10.1007/s12540-023-01438-2.

[5] J. Bai, Y. Yang, C. Wen, J. Chen, G. Zhou, B. Jiang, X. Peng, F. Pan, Applications of magnesium alloys for aerospace: A review, J. Magnes. Alloy. (2023). https://doi.org/10.1016/j.jma.2023.09.015.

[6] M. Easton, A. Beer, M. Barnett, C. Davies, G. Dunlop, Y. Durandet, S. Blacket, T. Hilditch, P. Beggs, Magnesium alloy applications in automotive structures, J. Occup. Med. 60 (2008) 57–62. https://doi.org/10.1007/s11837-008-0150-

8.

[7] S.H. Park, Y.J. Kim, H.J. Kim, S.C. Jin, J.U. Lee, A. Komissarov, K.S. Shin, Recent research progress on magnesium alloys in Korea: A review, J. Magnes. Alloy. (2023). https://doi.org/10.1016/j.jma.2023.08.007.

[8] S.J. Meng, H. Yu, S.D. Fan, Q.Z. Li, S.H. Park, J.S. Suh, Y.M. Kim, X.L. Nan, M.Z. Bian, F.X. Yin, W.M. Zhao, B.S. You, K.S. Shin, Recent Progress and Development in Extrusion of Rare Earth Free Mg Alloys: A Review, Acta Metall. Sin. (Engl. Lett.) 32 (2019) 145–168. https://doi.org/10.1007/s40195-018-00871-2.

[9] C. Cheng, Q. Lan, A. Wang, Q. Le, F. Yang, X. Li, Effect of Ca Additions on Ignition Temperature and Multi-Stage Oxidation Behavior of AZ80, Metals 8 (10) (2018) 766. https://doi.org/10.3390/met8100766.

[10] S.C. Jin, J.W. Cha, J. Go, J.H. Bae, S.H. Park, Comparative study of extrudability, microstructure, and mechanical properties of AZ80 and BA53 alloys, J. Magnes. Alloy. 11 (1) (2023) 249–258. https://doi.org/10.1016/j.jma.2021.07.009.

[11] S.C. Jin, J.W. Cha, S.H. Joo, S.H. Park, Enhancing tensile strength and ductility of high-speed-extruded Mg–5Bi–2Al through trace Mn addition, Mater. Charact. 181 (2021) 111500. https://doi.org/10.1016/j.matchar.2021.111500.

[12] J.W. Cha, S.C. Jin, S.H. Park, Microstructure and Mechanical Properties of Very-high-speed Extruded Mg–Bi–Al–Mn Alloy, Trans. Mater. Process. 31 (2) (2022) 73–80. https://doi.org/10.5228/KSTP.2022.31.2.73.

[13] J.W. Cha, S.C. Jin, J.G. Jung, S.H. Park, Effects of homogenization

temperature on microstructure and mechanical properties of high-speed-extruded Mg–5Bi–3Al alloy, J. Magnes. Alloy. 10 (10) (2022) 2833–2846. https://doi.org/10.1016/j.jma.2021.07.007.

[14] J. Go, S.C. Jin, H. Kim, H. Yu, S.H. Park, Novel Mg–Bi–Al alloy with extraordinary extrudability and high strength, J. Alloys Compd. 843 (2020) 156026. https://doi.org/10.1016/j.jallcom.2020.156026.

[15] J.W. Cha, S.C. Jin, S.H. Park, Microstructure and High-Cycle Fatigue Properties of High-Speed-Extruded Mg-5Bi-3Al Alloy, Trans. Mater. Process. 31 (5) (2022) 253–260. https://doi.org/10.5228/KSTP.2022.31.5.253.

[16] S.C. Jin, J.W. Cha, J.H. Bae, H. Yu, S.H. Park, Effects of Al addition on microstructure and mechanical properties of extruded Mg–3Bi alloy, J. Magnes. Alloy. 10 (7) (2022) 1887–1898. https://doi.org/10.1016/j.jma.2020.11.003.

[17] J. Go, J.H. Lee, H. Yu, S.H. Park, Significant improvement in the mechanical properties of an extruded Mg–5Bi alloy through the addition of Al, J. Alloys Compd. 821 (2020) 153442. https://doi.org/10.1016/j.jallcom.2019.153442.

[18] H. Mirzadeh, Grain refinement of magnesium alloys by dynamic recrystallization (DRX): A review, J. Mater. Res. Technol. 25 (2023) 7050–7077. https://doi.org/10.1016/j.jmrt.2023.07.150.

[19] F.J. Humphreys, M. Hatherly, Recrystallization and Related Annealing Phenomena, Elsevier, Oxford, 2004 second ed..

[20] S.C. Jin, J.U. Lee, J. Go, H. Yu, S.H. Park, Effects of Sn addition on the microstructure and mechanical properties of extruded Mg–Bi binary alloy, J. Magnes. Alloy. 10 (3) (2022) 850–861.

https://doi.org/10.1016/j.jma.2021.04.015.

[21] Y.J. Kim, J.U. Lee, Y.M. Kim, S.H. Park, Microstructural evolution and grain growth mechanism of pre-twinned magnesium alloy during annealing, J. Magnes. Alloy. 9 (4) (2021) 1233–1245. https://doi.org/10.1016/j.jma.2020.11.015.

[22] N. Tahreen, D.F. Zhang, F.S. Pan, X.Q. Jiang, D.Y. Li, D.L. Chen, Strengthening mechanisms in magnesium alloys containing ternary I, W and LPSO phases, J. Mater. Sci. Technol. 34 (7) (2018) 1110–1118. https://doi.org/10.1016/j.jmst.2017.12.005.

[23] W.L. Cheng, Q.W. Tian, H. Yu, H. Zhang, B.S. You, Strengthening mechanisms of indirect-extruded Mg–Sn based alloys at room temperature, J. Magnes. Alloy. 2 (4) (2014) 299–304. https://doi.org/10.1016/j.jma.2014.11.003.

[24] H.E. Friedrich, B.L. Mordike, Magnesium Technology, Springer, 2006.

[25] D.J. Bailey, W.F. Flanagan, Philos. Mag. 15 (1967) 43–49. https://doi.org/10.1080/14786436708230350.

[26] P.O. Guglelmi, M. Ziehmer, E.T. Lilleodden, On a novel strain indicator based on uncorrelated misorientation angles for correlating dislocation density to local strength, Acta Mater. 150 (2018) 195–205. https://doi.org/10.1016/j.actamat.2018.03.009.

[27] D.J. Child, G.D. West, R.C. Thomson, Assessment of surface hardening effects from shot peening on a Ni-based alloy using electron backscatter diffraction techniques, Acta Mater. 59 (12) (2011) 4825–4834. https://doi.org/10.1016/j.actamat.2011.04.025.

[28] S. Mandal, P.V. Sivaprasad, V.S. Sarma, Dynamic recrystallization in a Ti modified, austenitic stainless steel during high strain rate deformation, Mater. Manuf. Process. 25 (1–3) (2010) 54–59. https://doi.org/10.1080/10426910903162985.

[29] S. Mandal, A.K. Bhaduri, V.S. Sarma, A study on microstructural evolution and dynamic recrystallization during isothermal deformation of a Ti-modified austenitic stainless steel, Metall. Mater. Trans. A 42 (2011) 1062–1072. https://doi.org/10.1007/s11661-010-0517-7.

[30] Y. Cao, H. Di, J. Zhang, J. Zhang, T. Ma, R.D.K. Misra, An electron backscattered diffraction study on the dynamic recrystallization behavior of a nickel–chromium alloy (800H) during hot deformation, Mater. Sci. Eng. A 585 (2013) 71–85. https://doi.org/10.1016/j.msea.2013.07.037.

[31] V.M. Miller, T.M. Pollock, Texture modification in a magnesium-aluminum-calcium alloy during uniaxial compression, Metall. Mater. Trans. A 47 (2016) 1854–1864. https://doi.org/10.1007/s11661-016-3351-8.

[32] X.Q. Yin, C.H. Park, Y.F. Li, W.J. Ye, Y.T. Zuo, S.W. Lee, J.T. Yeom, X.J. Mi, Mechanism of continuous dynamic recrystallization in a 50Ti-47Ni-3Fe shape memory alloy during hot compressive deformation, J. Alloys Compd. 693 (2017) 426–431. https://doi.org/10.1016/j.jallcom.2016.09.228.

[33] C.D. Barrett, A. Imandoust, A.L. Oppedal, K. Inal, M.A. Tschopp, H. El Kadiri, Effect of grain boundaries on texture formation during dynamic recrystallization of magnesium alloys, Acta Mater. 128 (2017) 270–283. https://doi.org/10.1016/j.actamat.2017.01.063.

[34] G. Wu, J. Yu, L. Jia, W. Xu, B. Dong, Z. Zhang, B. Hao, Microstructure and

Texture Evolution of Mg-Gd-Y-Zr Alloy during Reciprocating Upsetting-Extrusion, Materials 13 (21) (2020) 4932. https://doi.org/10.3390/ma13214932.

[35] A. Hadadzadeh, F. Mokdad, M.A. Wells, D.L. Chen, A new grain orientation spread approach to analyze the dynamic recrystallization behavior of a cast-homogenized Mg-Zn-Zr alloy using electron backscattered diffraction, Mater. Sci. Eng. A 709 (2018) 285–289. https://doi.org/10.1016/j.msea.2017.10.062.

[36] M.R. Barnett, Twinning and the ductility of magnesium alloys: Part II. “Contraction” twins, Mater. Sci. Eng. A 464 (1–2) (2007) 8–16. https://doi.org/10.1016/j.msea.2007.02.109.

[37] D. Ando, J. Koike, Y. Sutou, Relationship between deformation twinning and surface step formation in AZ31 magnesium alloys, Acta Mater. 58 (13) (2010) 4316–4324. https://doi.org/10.1016/j.actamat.2010.03.044

[38] L. Lu, T. Liu, Y. Chen, Z. Wang, Deformation and fracture behavior of hot extruded Mg alloys AZ31, Mater. Charact. 67 (2012) 93–100. https://doi.org/10.1016/j.matchar.2012.02.023.

[39] M.R. Barnett, Z. Keshavarz, A.G. Beer, D. Atwell, Influence of grain size on the compressive deformation of wrought Mg–3Al–1Zn, Acta Mater. 52 (17) (2004) 5093–5103. https://doi.org/10.1016/j.actamat.2004.07.015.

[40] M.A. Meyers, O. Vöhringer, V.A. Lubarda, The onset of twinning in metals: a constitutive description, Acta Mater. 49 (19) (2001) 4025–4039. https://doi.org/10.1016/S1359-6454(01)00300-7.

[41] C. Wagner, G. Laplanche, Effect of grain size on critical twinning stress and work hardening behavior in the equiatomic CrMnFeCoNi high-entropy alloy,

Int. J. Plast. 166 (2023) 103651. https://doi.org/10.1016/j.ijplas.2023.103651.

Declaration of interests

☒ The authors declare that they have no known competing financial interests or personal relationships that could have appeared to influence the work reported in this paper.

☐The authors declare the following financial interests/personal relationships which may be considered as potential competing interests: